Lossless 3D FDTD of a 180-degree Hybrid Coupler: Extraction of Network Parameters

Ian Dwyer, *EE Student at University of Colorado Denver*

***Abstract* - There is very little error in MoM simulation in Keysight's ADS (Advances Design Systems), so the quality of a raw code developed for MathWorks' MATLAB 3-dimensional FDTD (Finite Difference Time Domain) approximation program designed is compared to a matching model in ADS using the MoM (Method of Moments) approximation obtaining network parameters for a microstrip design. The network parameters routine was developed using a skeleton lossless accelerated FDTD update code provided by Dr Stephen Gedney at the University of Colorado Denver with a PML layer included. A 3GHz 180-degree hybrid coupler microstrip is designed in each program for the experiment. The device's response is simulated using a 20GHz bandwidth Gaussing pulse due to its relatively flat response at frequencies much lower than the corner frequency of the pulse. Space was discretized to 9 mil per sample with isotropic steps, but anisotropic scaling for z direction components, between the discrete step sizes of the x-y plane and the z plane due to the z plane requiring a step size of 1.37 mil for the microstrip traces. The time was calculated to provide at least four reflections from the furthest location at the opposite port. Object oriented programming was implemented to aid in the process of design a post-processing to simplify construction and readily obtain values associated with object characteristics. Both models use lossless media definitions and use PEC conductor definitions. The quality of the FDTD algorithm is determined by its second order accuracy and makes it ideal for applications where high precision is required. The time domain FDTD model was found to require substantially longer calculation times than the frequency domain MoM model. The relative difference provided a maximum absolute difference of 10 dB with the FDTD at the operating frequency. The reflection was the largest error for all outputs at the operating frequency with the second largest error at the lobes of all traces. Error is lowest across the band at the opposite, through ports with no more than 10% error at any point. The error was generally 5% or a little greater in most aspects across the band providing that there are likely errors in the design of the FDTD program. There were troubles with scaling the voltages after the Fourier transforms and finding the effective permittivity of the substrate but is believed to have been solved. Despite the error margins observed, given the frequency accuracy and this model appears to be usable for less sensitive designs.**

***Index Terms* - FDTD, microstrip, network parameters, electromagnetics, 180-degree hybrid coupler, scattering parameters, MATLAB, Advanced Design Systems.**

I. Introduction

An EM (Electromagnetics) simulator that can generate network parameters provides an essential tool in microwave circuit design. The EM simulation provides field interactions in which Spice does not consider for higher precision requirements. Network parameters allow for interconnecting various devices at design frequencies between ports and knowing their expected interactions without need for simulating larger, more complex circuit architectures. Various numerical methods exist for EM simulation such as MoM (Method of Moments), FEM (Finite Electromagnetic), and FDTD (Finite-Difference Time-Domain) where FDTD is the only method intuitive with respect to traditional forms of Maxwell's equations with its technique being modular to any function, not only Maxwell's (such as for Schrodinger's wave equations), that requires differential operators to achieve second order accuracy for any required design precision with RAM and execution time as the limiting factors. In the case of network parameters, MoM is ideal for high-speed precision over limited frequency ranges and limited bins sampled as it uses linearized matrix operations best used for frequency domain operations such as the frequency dependent parameters in microwave circuits. Larger frequency bands with high resolution and fine meshing substantially slows MoM execution times. Despite MoM being a strong tool for PCB design, it is not suited for transient time-dependent EM simulations. The goal of this article is to show the ability of FDTD to not only produce a transient signal probable at any time or space point, but this time signal can be used for the frequency domain analysis which MoM are more heavily constrained to. Spice is used for time domain simulations but lacks EM capabilities of the previously mentioned numerical methods, regardless the results from the ADS Spice simulation are also provided for reference to compare the various solvers on Keysight's ADS available for obtaining network parameters.

What makes the FDTD unique is the explicit use of the function by using CDA (Central Differencing Approximation) instead of discrete forward or reverse differentiation so that all calculations occur from a shared point in time and space in which it is offset from, thus providing predictable spatial phase error to a square of its domain given the unknown area to another discrete point is a half-step box, entire based on the designers choice for any scale. To elaborate, the sample domain is represented by the Yee cells, both a secondary and a primary cell where they each represent Faraday's and Ampere's laws enacting in somewhat of a potential space, where half-step offsetting of these cells prevents violation of Maxwells laws while retaining minimum discretization error. Each cell is normal to the other where the primary and secondary cells have 50% overlap to transfer the fields with respect to Poynting's which provides the power definition where magnetic and electric fields operate orthogonally to each other and travel in the

direction of the power vector in which all three fields are orthogonal in relation. The program's functions from entire field updates occurring for each time step where the change in signal over that time produces a certain transient propagation over space with the explicit equations.

The FDTD in this article uses a 3D Maxwell update simulated in MATLAB R2022B with a PML (Perfectly Matched Layer) in lieu of ABCs (Absorbing Boundary Conditions) to reduce the domain and computation time. The number of time steps increase cubically for each discrete spatial step added for the DUT (Device Under Test) where planes must be added when increasing the mesh domain or when the mesh is made finer. The PML allows for reduction of the evanescing region to only be 10 cells thick with a gap of 2 where no excitation or measurements were taken closer than this, 12 cells, from the PEC shield. The matched load conditions are simulated by grounding the circuit through the PML which will act as an industry standard 50Ω matched network. The final design utilizes inhomogeneous permittivity between the free space and the substrate, but a homogenous substrate, in an isotropic update, but with scale z direction components (35), for the discrete spatial steps in the physical domain. The program is accelerated by normalizing the functions with the edge lengths (20) for the electric field and free space impedance for the magnetic fields. The physical domain is encased with a PEC (Perfect Electrical Conductor) which acts as shielding and a grounding plane for the system. The update is lossless, so substrate and atmospheric conductance and resistance losses are omitted from not only the FDTD, but all numerical EM solvers through the article. The purpose of this article is to observe the characteristics of the circuit and system showing efficacy and similarity in accuracy of the FDTD program's design with consideration to professional design software.

II. FDTD Theory

To understand the application, first we will derive a single field, electric, with its plane traveling in a single direction, the z-direction. The source update is intrinsic to the derivation and is expanded from the main field update. Derivation of the FDTD's CDA-based update can start either using the curl operation or using finite integration but the finite integration allows intuitive derivation with respect to the Yee cell. Starting with the integral form of Amperes law to obtain the electric field update:

$$\oint_c \vec{H}_{xy} d\vec{l} = \iint_s \frac{\partial}{\partial t}(\vec{D}_z + \vec{J}_z) d\vec{s} = \oint_c \vec{H}_{xy} d\vec{l} = \iint_s \frac{\partial}{\partial t} \epsilon \vec{E}_z d\vec{s} + \iint_s \vec{J}_z d\vec{s} \quad (1)$$

Let's use any direction as the derivation method is the same for each other direction in which the field can travel. As z is the direction in which the voltage is probed for an XY-plane PCB, we will use a z-traveling update derivation for example. Given that it is z-directed, we know that the surface normal is composed of discrete segments, Δx and Δy, of a cubes side can be generalized in (2).

$$\vec{H}d\vec{s} \rightarrow \sum H\hat{x}\Delta x + \sum H\hat{y}\Delta y \tag{2}$$

And the z-facing vector normal to the cell's surface:

$$d\vec{l} = \Delta x \Delta y \hat{z} \tag{3}$$

Using the z-face of a secondary Yee cell with discrete sample location (i, j, k) centered inside the cell and half steps in any direction towards the z-face, we obtain:

$$\oint_c \vec{H}d\vec{l} = -H^n_{x_{i+\frac{1}{2},j,k+\frac{1}{2}}}\Delta x + H^n_{y_{i,j+\frac{1}{2},k+\frac{1}{2}}}\Delta y + H^n_{x_{i-\frac{1}{2},j,k+\frac{1}{2}}}\Delta x - H^n_{y_{i,j-\frac{1}{2},k+\frac{1}{2}}}\Delta y \tag{4}$$

Use central difference approximation to differentiate time for the electric field component:

$$\iint_s \frac{\partial}{\partial \mathrm{t}}\epsilon\vec{E}_z d\vec{s} + \iint_s \vec{J}_z d\vec{s} = \frac{\epsilon\left(E^{n+\frac{1}{2}}_{z_{i,j,k+\frac{1}{2}}} - E^{n-\frac{1}{2}}_{z_{i,j,k+\frac{1}{2}}}\right)\Delta x\Delta y}{\Delta t} + J^n_{z_{i,j,k+\frac{1}{2}}}\Delta x\Delta y \tag{5}$$

The value of FDTD can be seen in the below form where both time and space differences were obtained simultaneously without changing the position n. We obtain the discrete explicit differential:

$$\frac{\epsilon\left(E^{n+\frac{1}{2}}_{z_{i,j,k+\frac{1}{2}}} - E^{n-\frac{1}{2}}_{z_{i,j,k+\frac{1}{2}}}\right)\Delta x\Delta y}{\Delta t} + J^n_{z_{i,j,k+\frac{1}{2}}}\Delta x\Delta y = \left(H^n_{y_{i,j+\frac{1}{2},k+\frac{1}{2}}} - H^n_{y_{i,j-\frac{1}{2},k+\frac{1}{2}}}\right)\Delta y - \left(H^n_{x_{i+\frac{1}{2},j,k+\frac{1}{2}}} - H^n_{x_{i-\frac{1}{2},j,k+\frac{1}{2}}}\right)\Delta x \tag{6}$$

Then we obtain the discrete update form by rearranging:

$$E^{n+\frac{1}{2}}_{z_{i,j,k+\frac{1}{2}}} = \left(\frac{\Delta t}{\epsilon}\frac{\epsilon}{\Delta t}\right)E^{n-\frac{1}{2}}_{z_{i,j,k+\frac{1}{2}}} + \frac{\Delta t}{\epsilon}\left[\frac{\left(H^n_{y_{i,j+\frac{1}{2},k+\frac{1}{2}}} - H^n_{y_{i,j-\frac{1}{2},k+\frac{1}{2}}}\right)\Delta y}{\Delta x\Delta y} - \frac{\left(H^n_{x_{i+\frac{1}{2},j,k+\frac{1}{2}}} - H^n_{x_{i-\frac{1}{2},j,k+\frac{1}{2}}}\right)\Delta x}{\Delta x\Delta y} - \frac{J^n_{z_{i,j,k+\frac{1}{2}}}\Delta x\Delta y}{\Delta x\Delta y}\right] \tag{7}$$

With the resulting update equation:

$$E^{n+\frac{1}{2}}_{z_{i,j,k+\frac{1}{2}}} = E^{n-\frac{1}{2}}_{z_{i,j,k+\frac{1}{2}}} + \frac{\Delta t}{\epsilon}\left[\left(H^n_{y_{i+\frac{1}{2},j,k+\frac{1}{2}}} - H^n_{y_{i+\frac{1}{2},j,k-\frac{1}{2}}}\right)\Delta x^{-1} - \left(H^n_{x_{i+\frac{1}{2},j+\frac{1}{2},k}} - H^n_{x_{i+\frac{1}{2},j-\frac{1}{2},k}}\right)\Delta y^{-1} - J^n_{z_{i,j,k+\frac{1}{2}}}\right] \tag{8}$$

The current density generated soft source is updated using a Gaussian for its relatively flat response with a bandwidth that is much greater than the operating frequency of the DUT.

$$J^n_{z_{i,j,k+\frac{1}{2}}} = e^{-\left(\frac{t-t_0}{t_\omega}\right)^2} \tag{9}$$

$$BW = \frac{1}{\pi t_\omega} \tag{10}$$

Source injection for a soft source has no internal impedance and causes no interaction other than impressed charge to prevent distorting the lossless results. Due to not being differentiated in space the source update can be applied as a vector update in the MATLAB language separate of the main field updates to inject various types of sources and increase readability in the recursive spatial update. The source update is easiest to understand if (8) is ordered as it is in (11).

$$E^{n+\frac{1}{2}}_{z_{i,j,k+\frac{1}{2}}} + \frac{\Delta t}{\epsilon} J^n_{z_{i,j,k+\frac{1}{2}}} = E^{n-\frac{1}{2}}_{z_{i,j,k+\frac{1}{2}}} + \frac{\Delta t}{\epsilon}\left[\left(H^n_{y_{i+\frac{1}{2},j,k+\frac{1}{2}}} - H^n_{y_{i+\frac{1}{2},j,k-\frac{1}{2}}}\right)\Delta x^{-1} - \left(H^n_{x_{i+\frac{1}{2},j+\frac{1}{2},k}} - H^n_{x_{i+\frac{1}{2},j-\frac{1}{2},k}}\right)\Delta y^{-1}\right] \tag{11}$$

This derivation can be applied to each direction using the same methods for the electric field update. The magnetic field update can be obtained using the same method but starting with Faraday's integral form which is the dual to Amperes as:

$$\oint_c \vec{E}_{xy} d\vec{l} = \iint_s \frac{\partial}{\partial \mathrm{t}}(\vec{B}_z + \vec{M}_z) d\vec{s} \tag{12}$$

All updates obtained from the update method in (12) are provided in (13) through (19).

$$E^{n+\frac{1}{2}}_{x_{i+\frac{1}{2},j,k}} = E^{n-\frac{1}{2}}_{x_{i+\frac{1}{2},j,k}} + \frac{\Delta t}{\epsilon}\left[\left(H^n_{z_{i+\frac{1}{2},j,k+\frac{1}{2}}} - H^n_{z_{i+\frac{1}{2},j,k-\frac{1}{2}}}\right)\Delta y^{-1} - \left(H^n_{y_{i+\frac{1}{2},j+\frac{1}{2},k}} - H^n_{y_{i+\frac{1}{2},j-\frac{1}{2},k}}\right)\Delta z^{-1} - J^n_{x_{i+\frac{1}{2},j,k}}\right] \tag{13}$$

$$E^{n+\frac{1}{2}}_{x_{i+\frac{1}{2},j,k}} = E^{n-\frac{1}{2}}_{x_{i+\frac{1}{2},j,k}} + \frac{\Delta t}{\epsilon}\left[\left(H^n_{z_{i+\frac{1}{2},j,k+\frac{1}{2}}} - H^n_{z_{i+\frac{1}{2},j,k-\frac{1}{2}}}\right)\Delta y^{-1} - \left(H^n_{y_{i+\frac{1}{2},j+\frac{1}{2},k}} - H^n_{y_{i+\frac{1}{2},j-\frac{1}{2},k}}\right)\Delta z^{-1} - J^n_{x_{i+\frac{1}{2},j,k}}\right] \tag{14}$$

$$E^{n+\frac{1}{2}}_{y_{i,j+\frac{1}{2},k}} = E^{n-\frac{1}{2}}_{y_{i,j+\frac{1}{2},k}} + \frac{\Delta t}{\epsilon}\left[\left(H^n_{x_{i+\frac{1}{2},j+\frac{1}{2},k}} - H^n_{x_{i+\frac{1}{2},j-\frac{1}{2},k}}\right)\Delta z^{-1} - \left(H^n_{z_{i+\frac{1}{2},j,k+\frac{1}{2}}} - H^n_{z_{i+\frac{1}{2},j,k-\frac{1}{2}}}\right)\Delta x^{-1} - J^n_{y_{i,j+\frac{1}{2},k}}\right] \tag{15}$$

$$E^{n+\frac{1}{2}}_{z_{i,j,k+\frac{1}{2}}} = E^{n-\frac{1}{2}}_{z_{i,j,k+\frac{1}{2}}} + \frac{\Delta t}{\epsilon}\left[\left(H^n_{y_{i+\frac{1}{2},j,k+\frac{1}{2}}} - H^n_{y_{i+\frac{1}{2},j,k-\frac{1}{2}}}\right)\Delta x^{-1} - \left(H^n_{x_{i+\frac{1}{2},j+\frac{1}{2},k}} - H^n_{x_{i+\frac{1}{2},j-\frac{1}{2},k}}\right)\Delta y^{-1} - J^n_{z_{i,j,k+\frac{1}{2}}}\right] \tag{16}$$

$$H^{n+1}_{x_{i+\frac{1}{2},j,k}} = H^n_{x_{i+\frac{1}{2},j,k}} + \frac{\Delta t}{\mu}\left[\left(E^{n+\frac{1}{2}}_{z_{i+\frac{1}{2},j,k+\frac{1}{2}}} - E^{n+\frac{1}{2}}_{z_{i+\frac{1}{2},j,k-\frac{1}{2}}}\right)\Delta y^{-1} - \left(E^{n+\frac{1}{2}}_{y_{i+\frac{1}{2},j+\frac{1}{2},k}} - E^{n+\frac{1}{2}}_{x_{i+\frac{1}{2},j-\frac{1}{2},k}}\right)\Delta z^{-1} - M^{n+\frac{1}{2}}_{x_{i+\frac{1}{2},j,k}}\right] \tag{17}$$

$$H^{n+1}_{y_{i,j+\frac{1}{2},k}} = H^n_{y_{i,j+\frac{1}{2},k}} + \frac{\Delta t}{\mu}\left[\left(E^{n+\frac{1}{2}}_{z_{i+\frac{1}{2},j,k+\frac{1}{2}}} - E^{n+\frac{1}{2}}_{z_{i+\frac{1}{2},j,k-\frac{1}{2}}}\right)\Delta x^{-1} - \left(E^{n+\frac{1}{2}}_{x_{i+\frac{1}{2},j+\frac{1}{2},k}} - E^{n+\frac{1}{2}}_{x_{i+\frac{1}{2},j-\frac{1}{2},k}}\right)\Delta z^{-1} - M^{n+\frac{1}{2}}_{y_{i,j+\frac{1}{2},k}}\right] \tag{18}$$

$$H^{n+1}_{z_{i,j,k+\frac{1}{2}}} = H^n_{z_{i,j,k+\frac{1}{2}}} + \frac{\Delta t}{\mu}\left[\left(E^{n+\frac{1}{2}}_{x_{i+\frac{1}{2},j+\frac{1}{2},k}} - E^{n+\frac{1}{2}}_{x_{i+\frac{1}{2},j-\frac{1}{2},k}}\right)\Delta y^{-1} - \left(E^{n+\frac{1}{2}}_{y_{i+\frac{1}{2},j,k+\frac{1}{2}}} - E^{n+\frac{1}{2}}_{y_{i+\frac{1}{2},j,k-\frac{1}{2}}}\right)\Delta x^{-1} - M^{n+\frac{1}{2}}_{z_{i,j,k+\frac{1}{2}}}\right] \tag{19}$$

The update coefficients are matrices matching the physical domain's dimensions to account for different material boundaries such as the substrate, free space and the PML boundaries. The Yee cell half-steps through the material with each step containing four material definitions to reduce error between updates with inhomogeneous boundaries. Material boundaries contained within a cell are averaged to ensure minimal discretization error at material boundaries between field exchanges on each update.

The output voltage signal was accumulated using (22) knowing the electric potential where the length is the number of series Yee cell edges, $N_k = k_b - k_a$, the discrete steps were in the z direction, $dl = dz = \Delta z$, the voltage probe was measuring (16).

$$V = -\int_{N_k} E dl \tag{20}$$

$$V = -\sum (k_b - k_a) E \Delta z \tag{21}$$

$$V = -\sum (N_k) E \Delta z \tag{22}$$

$$\frac{V}{\Delta z} = -\sum (N_k) \left(\frac{E_z(n + \frac{1}{2}, k)}{\Delta z} \right) \Delta z = -\sum (N_k) \left(e_z(n + \frac{1}{2}, k) \right) \Delta z \tag{23}$$

$$\vec{I} = \int_s \vec{J} ds = \oint \vec{H} dl \tag{24}$$

$$\vec{I} = \int_s \vec{J} ds = \sum [(H_{i+1}^n - H_i^n)\Delta x + (H_{k+1}^n - H_k^n)\Delta y] \tag{25}$$

It should be noted that in development, careful attention was paid to removing scaling from the accelerated code, so the voltages were never properly scaled until post processing. The z-probed voltages should have been scaled by dz (23) while current density, J, should have been solved for based on a desired input voltage. This could be causing some scaling issues and will be incoporated in future versions to initialize a desired voltage instead of desired current density.

Processing of the frequency domain information is done within each loop with the parallel processes optimized internal MATLAB Fourier transformation function, and stored for the final network parameter postprocessing once all ports have been tested for their modes. The FFT (Fast Fourier Transform) required 20GHz Gaussian for low gain error at 3GHz, but frequency discretization in the 3GHz region was very low at 600MHz per step. This was not acceptable so frequency domain interpolation was enforced by zeropadding the signal to obtain a number of FFT points to meet an acceptable discrete step size in the frequency domain which was increased with respect to the cubic nature of the space-time steps to ensure frequency bin accuracy using one for estimating the nececssary discretization (30) and another (27) for scaling the frequency domain signal's frequency and magnitude relation to the correct values. The final discretization used in the frequency domain had a resolution of 6.2MHz, which is still rather large but effective for the observation range.

Impedances were obtained by probing voltages and currents away from the source. Due to the orthogonality of voltage and current, voltage was obtained by testing along the z axis between the ground

and the trace while current was obtained by probing along the trace on either side of the voltage probe. To minimize phase error due to the true current being contained within the Yee cell, probing symmetrically on either side of the voltage probe, and multiplying the results and squaring that total produces a sort of product-averaging of the current phases along the voltage probe's cell edges. Ohms law in the frequency domain provided the frequency dependent impedances.

$$FFT\{x(n), N_{FFT}\} = \sum_{n=0}^{N-1} x(n) e^{-j\frac{2\pi n}{N_{FFT}}k} \tag{26}$$

$$X(k) = \frac{FFT\{x(n), N_{FFT}\}}{N_{FFT}} \tag{27}$$

$$N_{FFT_{min}} = 2^{12} \tag{28}$$

$$M = floor\{\log_2(N_t) - 12\} \tag{29}$$

$$N_{FFT} = 2^{3M} * N_{FFT_{min}} = 2^{3(\log_2(N_t)-12)+12} \tag{30}$$

Further postprocessing of the data is explained in the Program and Results section to consolidate references. Such information is the effective dielectric, line impedance, the scattering parameters, and the steps per wavelength with respect to stability.

III. The 180-degree Hybrid Coupler

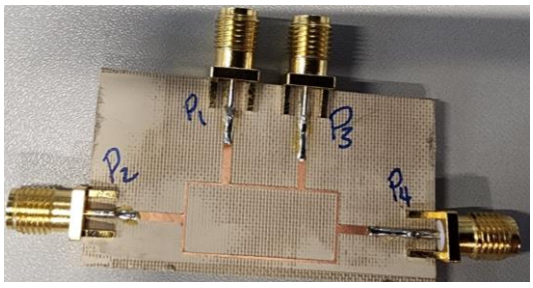

Fig. 1. Physical 180-degree hybrid coupler

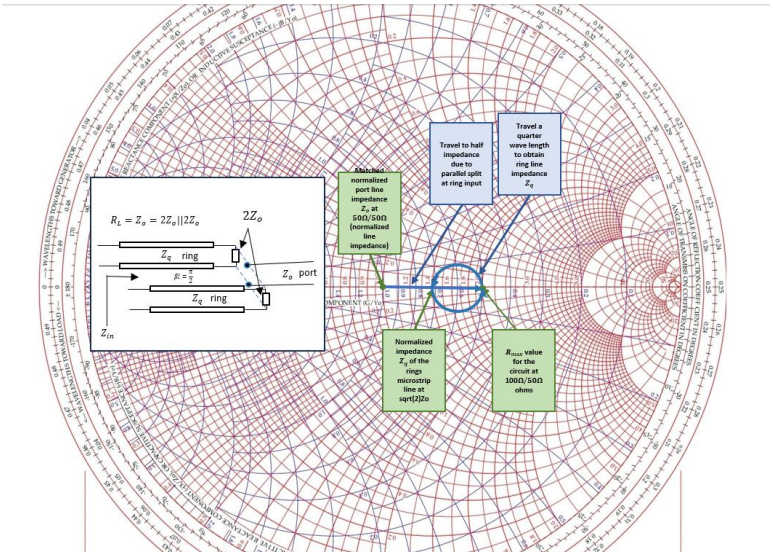

Fig. 2. Smith chart solution for ring impedance showing that impedance of thin ring is matched to ports.

The characteristic scattering matrix is found by using four ABCD matrices that each represent transmission line ABCD matrixes obtained from testing even and odd mode decomposition Fig. 3 as two ports are excited with various parings of half power excitations which are observed at the adjacent load on each of a split port where the split acts as either a short or open stub line. The scattering parameters are measured by testing the circuit by matching all ports and exciting each in a different simulation to obtain the through values. The data at the excited port will contain the initial pulse, seen in Fig. 13, so it was removed by using the reference line's data for a matching microstrip using (38).

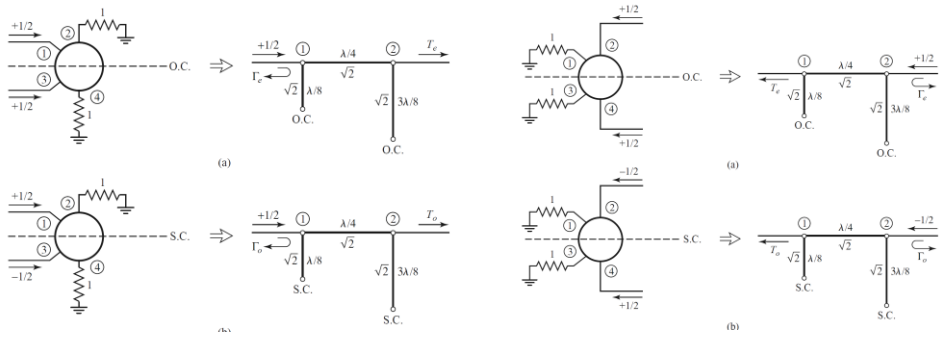

Fig. 3. Even-odd mode decomposition for a 180-degree hybrid divider. Figure 7.44-45 pg. 364-5 Pozar, D. M. (2012). Microwave engineering. Wiley.

From the scattering parameters (31) we can see from the ideal matrix that the 180-degree hybrid coupler is matched, reciprocal and lossless. It is matched as the sum of squares, which is essentially Parseval's, for any column or row result is one. It is lossless as the diagonal is zero, providing no reflection losses. It

is reciprocal as it has symmetry about the diagonal and thus is mirrored in the physical symmetry of the device. It delivers a phased signal, given the imaginary coefficient providing an electrical length of 90° lag and lead, evident by the complex coefficient in (31), in at either adjacent port with half of the power, also evident in (31) with a 3dB log-coefficient of root-two, delivered to these adjacent ports. The opposite port is always isolated ideally with an r_{max} of 100Ω and the reflection coefficients along the diagonal are zero providing the source has isolation from itself as well. The term 180-degree hybrid coupler comes from the understanding that the two ports that have power delivered to them are 180 degrees in electrical length apart with isolation ports having the same characteristic.

$$\frac{\vec{V}^-}{\sqrt{Z_o}} = -\frac{j}{\sqrt{2}}\begin{bmatrix}0 & 1 & 1 & 0\\ 1 & 0 & 0 & -1\\ 1 & 0 & 0 & 1\\ 0 & -1 & 1 & 0\end{bmatrix}\frac{\vec{V}^+}{\sqrt{Z_o}} \tag{31}$$

$$\vec{\boldsymbol{V}} = \begin{bmatrix}50 & 70.7 & 70.7 & 100\\ 70.7 & 50 & 100 & 70.7\\ 70.7 & 100 & 50 & 70.7\\ 100 & 70.7 & 70.7 & 50\end{bmatrix}\vec{\boldsymbol{I}} \tag{32}$$

Distance may be further understood as arctan's QI-QIV domain is -90° $< \beta l <$ 90° where power has the same delivery at any point 180-degrees away with power being enabled or disabled at a port every 90°.

$$\beta l = \frac{2\pi}{\lambda} * \frac{\lambda}{4} = \frac{\pi}{2} = 90° \tag{33}$$

This trait gives the 180-degree hybrid coupler unique applications such as coupling signals from the opposite ports to produce a full power mixed signal, and may also be used for other less efficient, due to half power loss, purposes such as reading from the unused signal port to monitor its opposite port's signal without disrupting the signal path. A physical version of the circuit can be seen in Fig. 1 for reference.

IV. Programs: MATLAB (FDTD) and ADS (MoM & Spice)

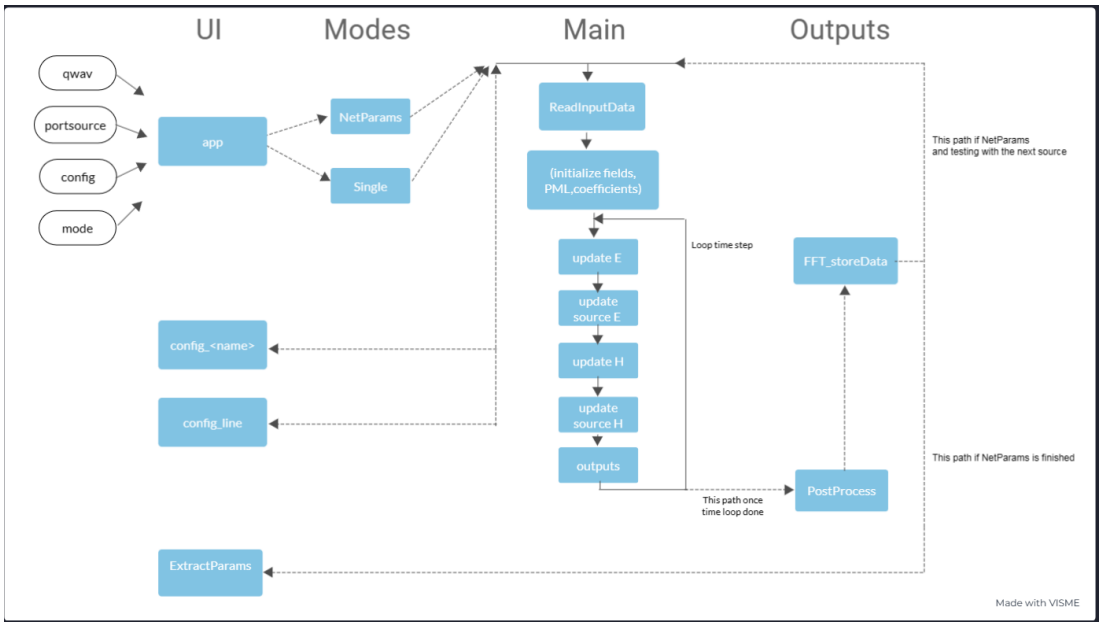

Fig. 4. Top level signal flow diagram of MATLAB FDTD application.

The network parameters routine was developed using a skeleton lossless FDTD code provided by Dr Stephen Gedney at the University of Colorado Denver and licensed for limited use. The code was accelerated using scaling relative to the field type and direction. Edges of the direction for electric fields and $\eta_o = \sqrt{\frac{\epsilon_o}{\mu_o}}$ (where ϵ_o is free space permittivity and μ_o is free space permeability) for magnetic fields are used as the scaling factors with both being normalized by their respective dl. This reduces floating points carried for an approximate speedup of 20% which required rescaling back to the true magnitudes after the simulation in post-processing. The code contained a perfectly matched layer (PML) in lieu of ABCs for improved simulation times by reducing the simulated domain which provides a large improvement given the increase of sim time by $N -> N_t^3$ for O(NL) computations since the spatial iterations are cubic for each time step.

Due to the domain and simulation time issues the discrete spatial steps were carefully calculated. The discrete time steps Δx, Δdy and Δz were originally chosen for 20 steps per wavelength using the bandwidth of the Gaussian signal of $\frac{1}{\pi t_\omega} = 20GHz$ but this provided poor spatial step resolution. This resulted in a discretization of 27 mil per step which is larger than the lowest discretization required for recreating the traces. The Δx was then given the lowest common factor of Δy and Δx then Δz was scaled

for the 1.37 mil conductor which what likely made more possible than expected due to lower complexity in the z-direction.

$$dl_{scale} = 9\ [mil] \tag{34}$$

$$dl = \frac{dl_{scale}[mil]}{1000\left[\frac{mil}{in}\right]} * \frac{2.54\left[\frac{in}{cm}\right]}{100\left[\frac{cm}{m}\right]} = 0.23[mm] \tag{35}$$

This method was unfortunately very computationally intensive but appeared to produce the most accurate results but predictively had low error with reasonable simulation times.

Discrete steps in x and y are equal and six times the discrete steps in z to achieve the 1.37 mil conductor thickness with scaling applied to dx and dy. Effective values in all other areas are rounded to their nearest value which is divisible by the lowest common factor of 9 for scaling. This is due to the smallest trace being 18 mil and the next being 45 mil where discretization error would be largest. Values larger than 100 mil will each produce no more than $\frac{\frac{9}{2}\,mil}{100\,mil} = 0.045$ or 4.5% error at that point. All other values are above $380\ mil$, so error contributed by discretization if x and y directions have a maximum of 1.25% for each update.

For stability with respect to steps in space and time, we must use the stability criterion with a Courant number, CN, less than one but as close to one as possible for lowest phase error in the stability region. The CN was set to 0.99 to achieve this design requirement. The stability relation defines our time discretization with respect to space and shows how the updates interact in time-space, provided in (36).

$$dt = \frac{CN}{c_o\sqrt{\left(\frac{1}{dl_x}\right)^2 + \left(\frac{1}{dl_y}\right)^2 + \left(\frac{1}{dl_z}\right)^2}} \tag{36}$$

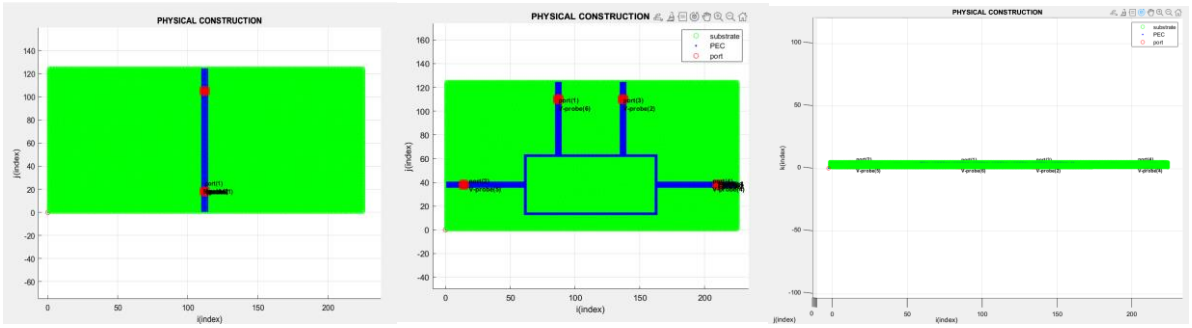

Fig. 5. (left) Graphical representation of the line used for reference impedance and forward voltage values. (center) The 180 hybrid PCB graphical view. (right) XZ-plane view of PCB for substrate height representation.

```
Simulation complete after  77.36 seconds
```

Fig. 6. Sample output of execution time from program between individual source tests.

The network parameters program first runs the equivalent line microstrip circuit, then runs the accelerated loop once for each each set of row parameters by shifting the excited port. This causes the function to be 5*O(LN) where a single program, O(LN) FDTD loop, averages 78 seconds. The entire network parameter extraction program executes in 6.5 minutes with a simulation time of one nanosecond, discrete step size in all directions of 0.23 millimeters, and a total of 2294 time samples to operate over a simulation domain of $\vec{N}_{xyz} = 145 * 85 * 17 = 209525$ spatial steps per time step. Execution time could be reduced by 40% by taking symmetry into account and only testing ports 1 and 2 or ports 3 and 4 and assuming reciprocal scattering matrix results, possibly reducing the execution time to 4 minutes. The MoM simulation executed in a single minute with discretiztion of 100 bins over 6GHZ, but as previously explained, MoM is best suited for paramter extraction due to using frequency domain linear matrix computations. To achieve the same 40GHz band and 368409 frequency bin discretization as the FDTD the MoM simulation required nearly 12 minutes which results in 160% increase in simulation time from the full FDTD program, and nearly being 300% greater simulation time than if the FDTD accounted for symmetry. This is a massive finding as a circuit designed for higher frequencies would be physically smaller, thus improving the efficiency of the FDTD and decreasing the efficiency of the MoM with devices that require large bands with high discretization.

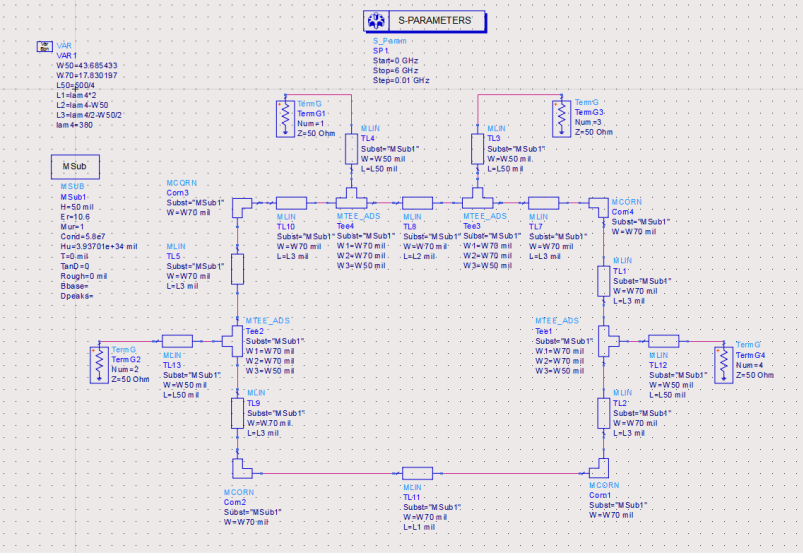

Fig. 7. ADS Spice model schematic.

For user manipulation, the program uses objects to be able to utlize output data without regeneration of the outputs and provides clear packaging of correlated traits. For more user fiendly navigation, the system uses various directories to consolidate processes. The program operates at any one point in a directory such as the loop without leaving until repretitive processes are completed to maintain speed. The jump into and out of a directory is done local to for stable use of navigating local directories between many cohesive files. Once any of the processes such as pre-processing, loop, or post-processing finishes, the program returns to main. The program avoids function calls to retain all values generated from a separate MATAB script which is set up similar to a function to aid in readability of process flow. This loads the workspace instead of returning values as a function would. If the program breaks while running, it has been designed to return to the programs root and rethrow the error without breaking the program for development purposes. The system also uses workspace saves to exchange data between the simulations before compiling all data to the final output objects. This further aids in retaining workspace data even if the program fails to aid in debugging. The program also uses visual aid of 3D scatter with all probe and ports objects marked to ensure funcionality of components as seen in Fig. 8 and provides an idea of the effective nature of using OOP for its specific usefulness in physical object orientation.

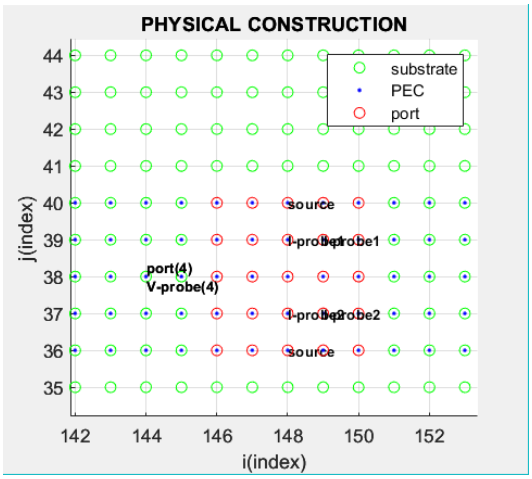

Fig. 8. Example of how ports are oriented with voltage probes, current probes, and the source across the port.

The object orientated PCB design files utilizes OOP (Object Oriented Programming) to allow the designer to describe the traces as length, width, heigth, and a reference location as seen in the far left in Fig. 9. The reference location is automatically converted from mils to samples for simplifying development procedures. The source is directly tied to the port location which is directly tied to a respective port's trace as it is adjusted where the location always remains 2 samples from the PML's terminating boundary. The probes are also directly connected to this port as traces are adjusted. A visual represetation of this

correlation can again be referenced in Fig. 8. This provides the user the ability to tune with line values after all objects have been effectively established with the structure method by using any config file as a template for the design. The output data is somewhat automatically generated, but some conditional relations are imposed such as how many ports and how those ports relate to the output data will likely need to be changed between different circuit designs. As a developmental note, it would be wise to use the script blocks as methods through a program class so that the objects are held in an FDTD application class. This would allow for consolidated toolboxes designed specifically for the format of the output data, providing a more intuititve interface resulting in faster debug and design.

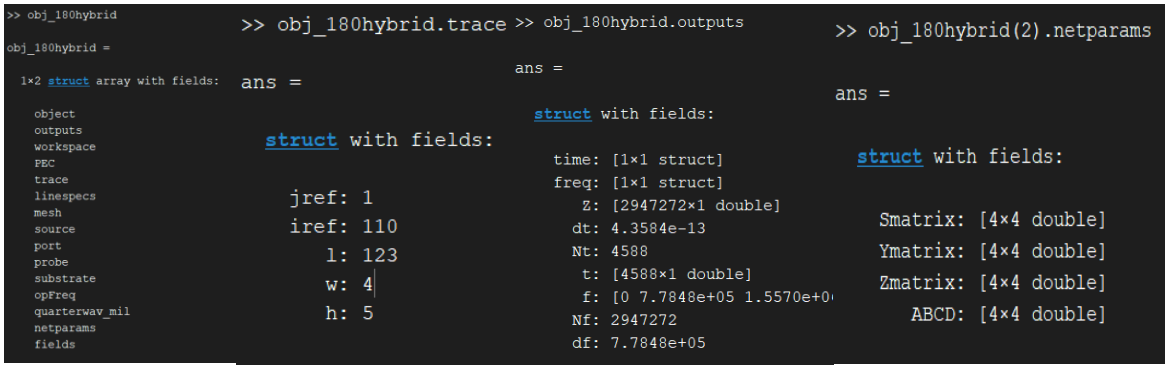

Fig. 9. (Left) Output object for MATLAB program for static user post processing and inspection. (Right) Trace object design showing definition of the trace as length, width, height, and reference coordinates. Object's sub-structures for outputs and network parameters.

For all condctor values used in the simulations their values were generated using the LineCalc tool in ADS by providing the material and design paramters to synthesize the physical dimensions of the trace. This method produces reliable results to use across all solvers for achieving the intended effective electrical angles and impedances Fig. 10. To achieve 50Ω ports, a width of 17.8 mil was used in ADS and 18 mil was used in the FDTD program. To achieve 70.7Ω ring line resistance with electrical length, $\beta l = 90°$, 43.69 mil width was used with a length of 384.63 mil length was used for the quarter wavelength distances in ADS with 45 mil widths and 380 mil lengths used in the FDTD program.

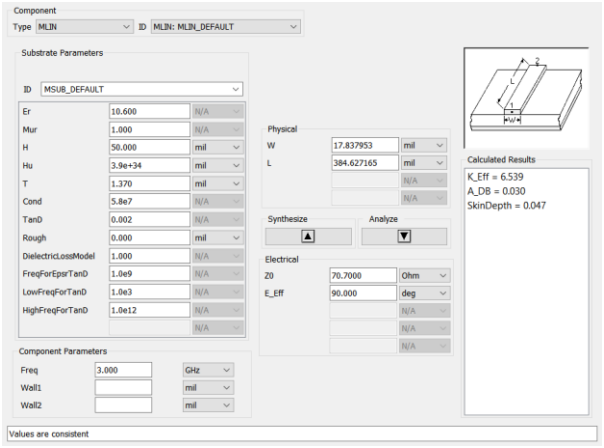

Fig. 10. Line calc tool used in ADS for finding lengths and widths of traces with respect to a desired impedance and substrate characteristics. The values obtained were used in the FDTD.

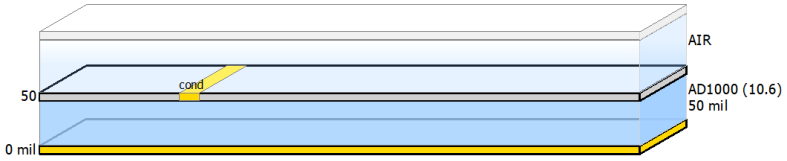

Fig. 11. Physical PCB substrate for MoM ADS design in the substrate editor.

In all three models, the substrate required the same definitions to match a Roger AD1000 substrate with characteristic values of importance being a dielectric constant of 10.6[F/m], a trace thickness of 1.37 mil and a substrate height of 50 mil using PEC traces without conductivity losses active on any solver. The Spice solver uses ‘msub’ as seen in Fig. 10, the MoM solver uses the substrate editor Fig. 11, and the FDTD substrate is setup within each user-defined config file in the root of the program with the other programs which require user interface.

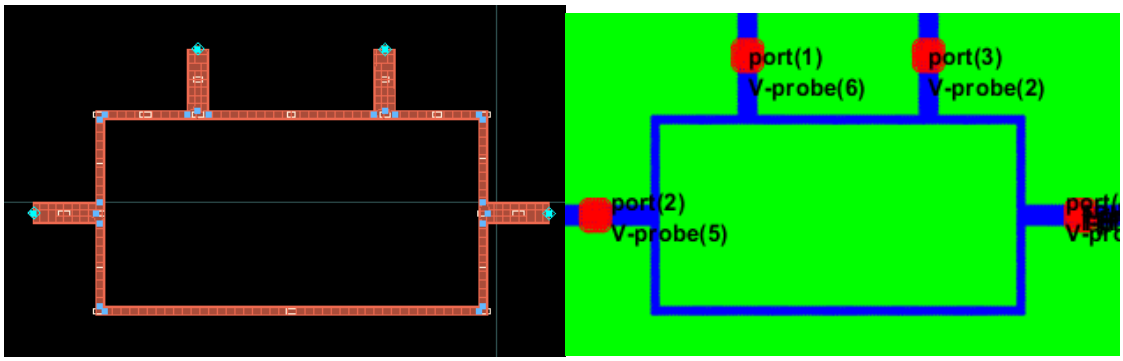

Fig. 12. Side-by-side view of the physical designs in ADS and MATLAB (to the left and right respectively).

V. Results: Analysis of Network Parameters Extracted

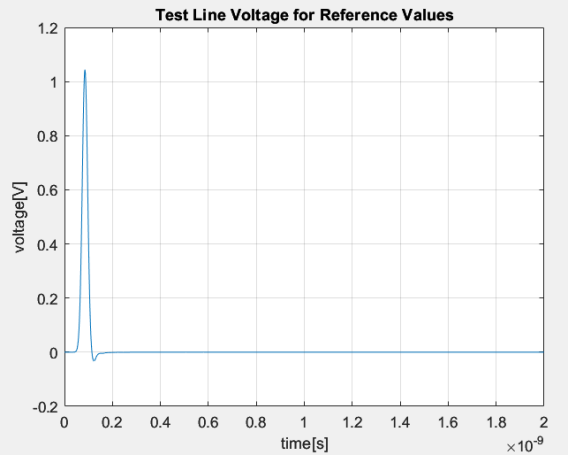

Fig. 13. Forward reference voltage signal used for obtaining reflection scattering parameters.

A key function of the network parameter extraction program to note for the following results is the voltage readouts at the source are a superposition of the forward and the reverse voltage signals. The source port contains the initial signal which must be removed from the probe located at the source port. Subtracting the forward signal obtained from the reference line voltage provided Fig. 13, used as the characteristic forward signal, any reflections back into that port after initialization will now be effectively represented since, we know there was no reverse signal before the pulse was initialized.

$$V(t,l) = V^{+}(t,l) + V^{-}(t,l) \tag{37}$$

$$V^{-}(t,l) = V(t,l) - V^{+}(t,l) \tag{38}$$

This was the only modification required to the output traces to obtain the desired trends, otherwise the reflection signal appears as though 100% of the signal is returned at the source port. The frequency domain transformations of the time domain voltage results in Fig. 14 are used to provide the scattering traces with the caveat of the return signal for source port 1 in that figure.

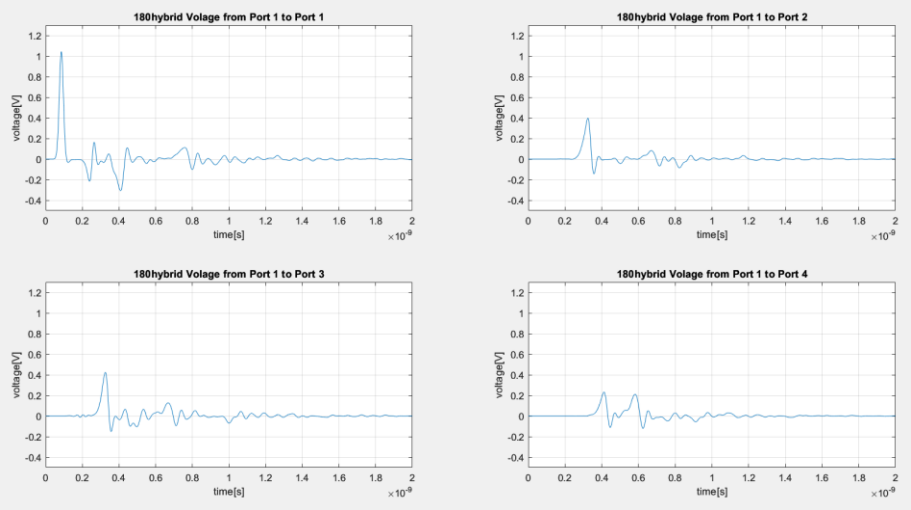

Fig. 14. Time domain voltage outputs testing with source at port 1 for the 180-degree hybrid coupler.

Result data was imported from an ADS model matching the construction made in MATLAB for the FDTD model. Interpolation of the ADS data was required due to higher resolution in the MATLAB frequency domain data and constriction of the domain was made on the FDTD data due to the MoM data being constrained from 0 to 6GHz. A comparison was made to determine the quality of the lossless FDTD network parameter simulator using the professionally designed MoM solver as the control.

The frequency domain results of the FDTD solver after removing the source signal from its respective probe can be seen in Fig. 15 with an overlay of the results from the MoM solver with absolute error below the magnitude responses in Fig. 16 and the phase response in Fig. 17 where the left plots are the MoM results, and the right plots are the Spice results. With respect to the design parameters of the 180° hybrid coupler had a operating frequency corner error of 91.58MHz at 2.9084MHz, a relative design error of 3.05%, where the scattering parameter matrices shown in (40) are pulled from the sample closest to the 3GHz design corner and do not reflect the true corner of the measured device's characteristic corner. Despite this, the values between each model retrieved at the design operating frequencies parameters match well with good bandwidths. The FDTD isolation bandwidth is slightly narrower but is still a broadband device with near 50% bandwidth at all through and isolation ports.

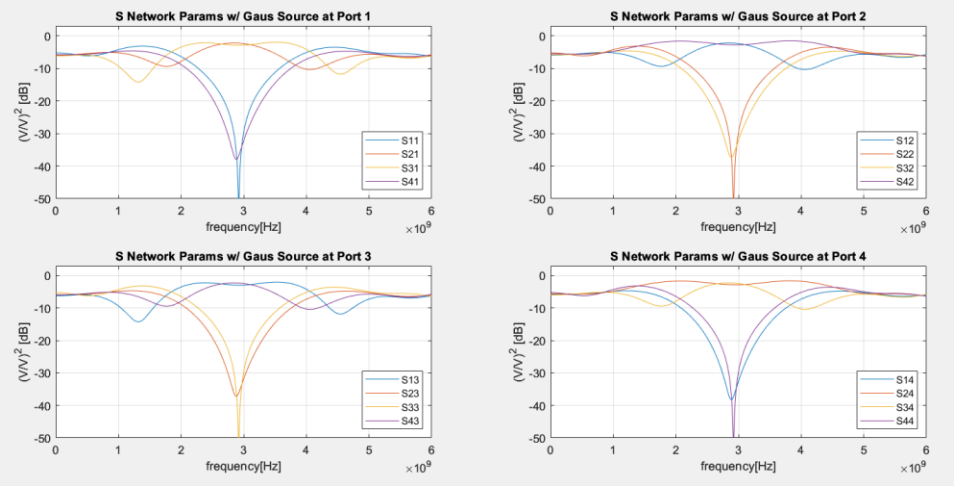

Fig. 15. Frequency domain voltage outputs testing with source at port 1 for the 180-degree hybrid coupler.

Results show likely probing error given the 4% gain above half power for S34, S43, S12 and S21. This is later speculated and quantified as a likely being phase error extracted from traces in Fig. 15 to obtain minimunm, mean and max phase error with assuming the MoM solver is designed well enough to use as a design reference. Some error, including the phase error, could be discretization error in the port spacing due to the 9-mil step size in physical placement. Simulation required three hours in previous testing for discretization of 1 mil, so this hypothesis has not been tested. High lobes on return loss traces are a further indicator of the phase error incurred in design. The lobe distortion as frequencies increase could be due to not effectively removing the forward signal from ports which were not oriented in the same direction as the reference line's signal or if sampling was slightly off to cause a time shift which would prevent proper removal of the forward signal and appear as a phase delay. The probing error visible at port 2 in the phase plots of Fig. 17 error is likely from subtracting the y-directed forward reference line voltage from the x-directed ports 2 or 4, where the signal is perpendicular to the reference used, producing phase error in measurement. Debugging this will likely result in substantially improved results. The absolute difference in the time domain magnitude is used to quantify the magnitude error visible in Fig. 16since the Gaussian-based signals observed should be between zero and one within the frequency range observed, therefore absolute difference provides a clear difference in outputs due to the normalized nature of the output signals for unity gain. There was max variation of 20% between the Spice and FDTD models with a mean of 5%. There was a max variation of 10% between the MoM and FDTD models with a mean of 5%. The results between MoM and FDTD are of highest interest due to both being the EM simulations.

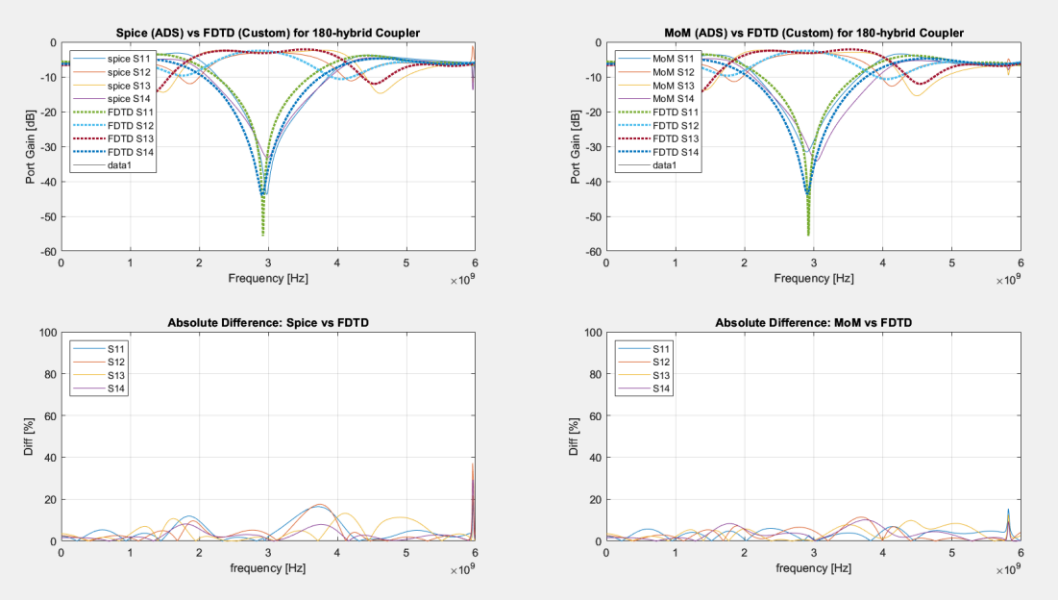

Fig. 16. FDTD and MoM comparison in frequency domain. Left is the magnitude spice comparison and right are the MoM comparison both generated by ADS.

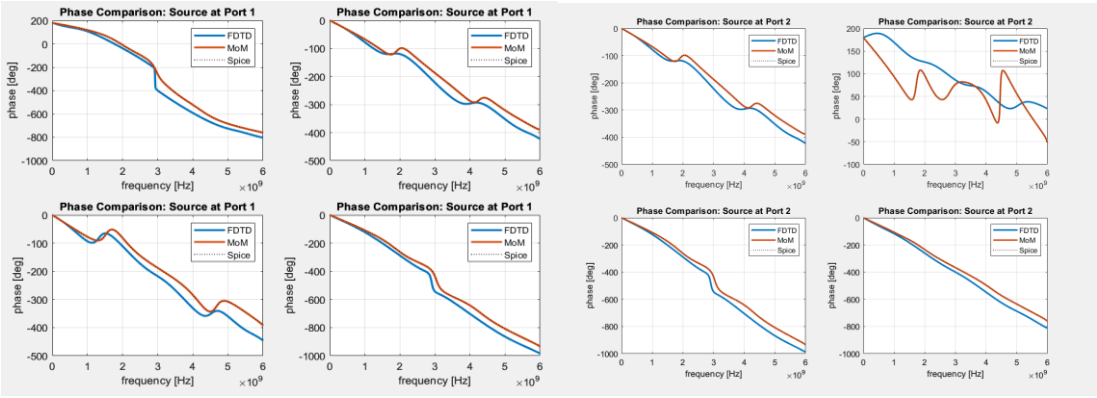

Fig. 17. Phase plots. Unwrapped phase responses for all solvers with ports 1 (left) and 2 (right) excited. Due to symmetry only 2 ports shown.

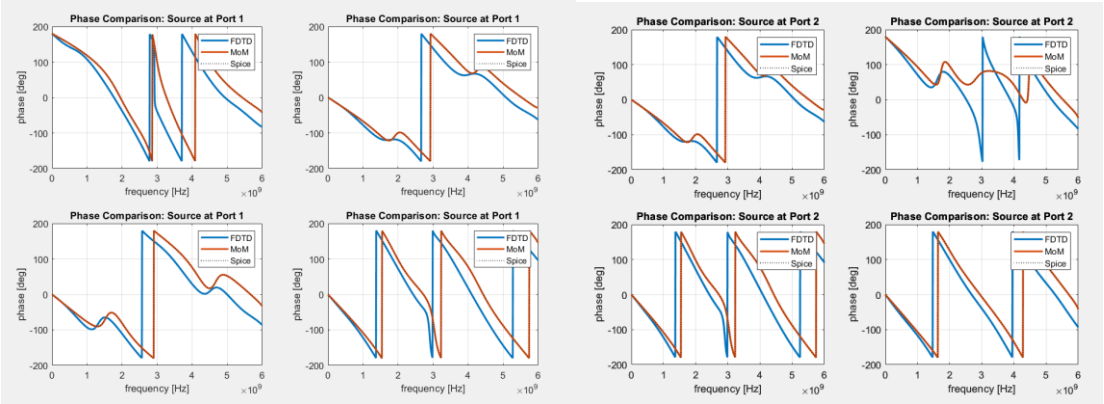

Fig. 18. Wrapped phase response for all solvers with source at ports 1 (left) and 2 (right).

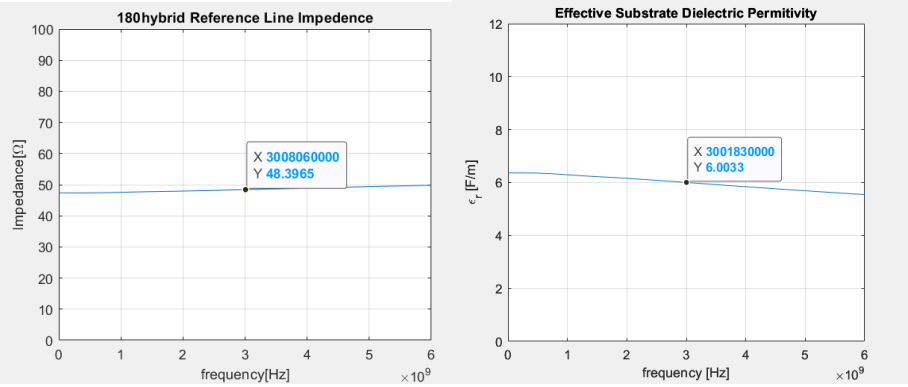

Fig. 19. (left) Line impedance obtained from reference line for port voltage calculations. (right) Effective dielectric of substrate for FDTD solver.

Frequency dependent line impedance on left, depicted in Fig. 19, was obtained by taking a voltage signal 36 mil, 4 samples, from the source across parallel z direction blocks with two parallel 9 mil blocks of current in the orthogonal direction along the trace for the current where we apply Ohm's law in the frequency domain,

$$\tilde{\mathrm{Z}}_{\mathrm{o}}(f) = \frac{\tilde{V}(f)}{\sqrt{\tilde{I}_2(f) * \tilde{I}_1(f)}}. \tag{39}$$

$$[\vec{V}] = \begin{bmatrix} 51.65 & 68.99 & 72.71 & 99.35 \\ 69.17 & 52.2 & 99.51 & 73.2 \\ 72.73 & 99.35 & 51.5 & 68.99 \\ 99.52 & 73.2 & 69.15 & 52.32 \end{bmatrix} [\vec{I}] \tag{40}$$

$$Z_{o_{hybrid}}^{FDTD} = 52\Omega \tag{41}$$

$$Z_{o_{line}}^{FDTD} = 48.4\Omega \tag{42}$$

$$Z_o^{MoM} = Z_o^{spice} = 50\Omega \tag{43}$$

The port impedances are seen in the Z-matrix, (40), across the diagonal, root-two times the port impedance at all adjacent port and r_{max} along the reciprocal diagonal. There were troubles obtaining reasonable values for all port impedance probes, so the matrix was obtained using MATLAB's internal $s2z(S, Z_o)$ function using the operating frequency scattering matrix obtained from voltages and previously obtained line impedance of 48.4Ω, (42), with reasonable results. The admittance matrix is also stored in the final object as the matrix inverse of the impedance matrix. The MoM and Spice produced 50Ω at all port, which provides some of the FDTD error is likely due to discretization error in the port widths producing conditions which are not fully matched.

Using FFT and Ohms law with the root product of the currents for reduced phase error due to offset voltage and current edges we obtain the complex frequency dependent line impedance vector, $\tilde{\mathrm{Z}}_{\mathrm{o}}(f)$. The effective permittivity, right-most plot in Fig. 19, was obtained knowing the continuous somewhat lossless expression for the wave number (44),

$$\beta = \frac{\omega}{v}\left[\frac{rad}{m}\right]. \tag{44}$$

The effective wave number, β_{meas}, can be used to find the effective relative dielectric permittivity after simplifying for $\epsilon_{r_{eff}}$ using (45)

$$\beta_{meas} = \omega\sqrt{\mu\epsilon_o\boldsymbol{\epsilon_{r_{eff}}}} = -\frac{angle\left\{\frac{\tilde{V}(f,l+m)}{\tilde{V}(f,l)}\right\}}{(l+m)-l}. \tag{45}$$

$$m = distance\ offset\ beteen\ probes\ in\ meters$$

$$c_o = \frac{1}{\sqrt{\mu_r\mu_o\epsilon_o}} = \frac{1}{\sqrt{\mu_o\epsilon_o}} \tag{46}$$

$$\boldsymbol{\epsilon_{r_{eff}}} = \left(\frac{angle\left\{\frac{\tilde{V}(f,l+m)}{\tilde{V}(f,l)}\right\}}{m\omega c_o}\right)^2 \tag{47}$$

ADS obtained an ideal line impedance of 50Ω and an effective ϵ_r of $6.54\left[\frac{F}{m}\right]$ compared to the FDTD's 48.4Ω and $6\left[\frac{F}{m}\right]$ respectively. For the general dielectric permittivity, we have a wavelength of (48),

$$\lambda_{sub} = \frac{2\pi}{\beta} = \frac{2\pi}{\omega\sqrt{\mu\epsilon_o\boldsymbol{\epsilon_r}}} = \frac{1}{f\sqrt{\mu\epsilon_o\boldsymbol{\epsilon_r}}} = \frac{c_o}{f}\frac{1}{\sqrt{\boldsymbol{\epsilon_r}}} = \frac{\lambda_o}{\sqrt{\boldsymbol{\epsilon_r}}} = 0.0297[m]. \tag{48}$$

The effective wavelength is closer to the response (49),

$$\lambda_{eff} = \frac{2\pi}{\beta_{meas}} = \frac{\lambda_o}{\sqrt{\boldsymbol{\epsilon_{r_{eff}}}}} = 0.0395[m]. \tag{49}$$

We obtain an steps per wavelength through the substrate at double the operating frequency as this is the band range to permit and isolate signals within, so the wavelengths are effectively halved to represent the entire range and will use the smallest wavelength for worst case purposes of λ_{sub} providing 64 steps per wavelength resolution which should provide more than adequate results given the generally accepted minimum of 20 steps per wavelength.

$$N_{\frac{dl}{\lambda}} = \frac{\frac{\lambda_{sub}}{2}}{dl} = \frac{0.015[m]}{0.23[mm]} = 64\left[\frac{N_l}{\lambda}\right]$$

Comparing the scattering matrices, line impedances, and effective dielectric permittivity at the operating frequency it is apparent that there are some design flaws, but that the parameters are similar enough to generally say that the FDTD program could function for low-accuracy designs with similar considerations represented in this article to each design.

$$\frac{\left[\vec{V}^{-}_{FDTD}(3[GHz])\right]}{\sqrt{48.39}} = -\frac{j}{\sqrt{2}}\begin{bmatrix}0.04 & 1.04 & 0.98 & 0.02\\ 1.04 & 0.04 & 0.02 & -0.99\\ 0.98 & 0.02 & 0.04 & 1.04\\ 0.02 & -0.99 & 1.04 & 0.04\end{bmatrix}\frac{\left[\vec{V}^{+}_{FDTD}(3[GHz])\right]}{\sqrt{48.39}} \tag{50}$$

$$\frac{\left[\vec{V}^{-}_{MoM}(3[GHz])\right]}{\sqrt{48.39}} = -\frac{j}{\sqrt{2}}\begin{bmatrix}0.05 & 0.97 & 0.98 & 0.03\\ 0.97 & 0.01 & 0.03 & -1\\ 0.98 & 0.03 & 0.05 & 0.97\\ 0.03 & -1 & 0.97 & 0.01\end{bmatrix}\frac{\left[\vec{V}^{+}_{MoM}(3[GHz])\right]}{\sqrt{48.39}} \tag{51}$$

$$\frac{\left[\vec{V}^{-}_{spice}(3[GHz])\right]}{\sqrt{48.39}} = -\frac{j}{\sqrt{2}}\begin{bmatrix}0.01 & 1 & 1 & 0.03\\ 1 & 0.07 & 0.03 & -1\\ 1 & 0.03 & 0.01 & 1\\ 0.03 & -1 & 1 & 0.07\end{bmatrix}\frac{\left[\vec{V}^{+}_{spice}(3[GHz])\right]}{\sqrt{48.39}} \tag{52}$$

The scattering parameters show a max of 7% difference in port parameters with a mean of 3% parameter-to-parameter. The line impedance provides 3.2% error in design. The effective dielectric measured at 3GHz, $6.0033\left[\frac{F}{m}\right]$, has 8.2% relative difference with respect to the LineCalc estimate, $6.539\left[\frac{F}{m}\right]$ in ADS. The reflection coefficients for each port exist where $i = j$ for $\bar{S}_{ij}$ along the matrix diagonal.

The error of 10% is likely due to discretization, probing orientation, source-type error, but such large amounts is not likely due to the phase error in the XY-direction as there are 64 steps per wavelength. Some phase error could be affecting the z-direction to the extent of 5% distortion as the scaling is nearly a sixth of the XY-direction where anisotropic scaling could distort some values. Phase error is one of the final important quantifiers of the quality of the program which also provides some frequency shift from the error. The reference for phase errors is from data in Fig. 17. The maximum mean phase error tested with the source at port 1 was -23° at port 4, minimum mean phase error was with the load at port 2 at 12°. The min error is 0 at DC with the lowest maximum phase error for port 1 source and port -30.8° and highest maximum phase error is with source at 1 and port 1 at -156°, nearly completely inverted phase, at the operating which further justifies that there is likely a better method to isolate or error in isolating the signals at the source ports or it could be strictly the mismatch in frequency due to frequency shifting. The result that he means were significantly lower indicates the trend of the error is likely closer to the mean

values with larger error at higher frequencies. Error could likely be reduced by increasing the corner of the pulse, reducing spatial step size, correcting the predictable error in phase using (ref # source), and fixing speculated probing errors.

VI. Summary of Project

The project had more suspected designer errors than expected but worked far better than expected for the errors that were found. Across the board, there appeared to be around a 7% design difference when compared comparing the ADS MoM solver with the MATLAB FDTD solver. This is found to be impressive as the signal meets so many locations where error could happen in the update due to design error, yet the essential specifications such as frequency, magnitude and phase characteristics maintain near a confidence of 93% functionality with larger errors generally at higher frequencies or near operating frequency due to unique characteristics of the device reaching only up to 80% confidence in design similarity to a Keysight ADS MoM simulation. If the developmental errors were corrected, then further sub-routines and features could be added as second order accuracy would be easier to quantify to validate the functionality. The developed program appears to be functional for very simple, low-resolution simulations that have low sensitivity. The network parameters program may be further developed by integrating more source types, using Thevenin sources to help represent unmatched devices paired, develop for lossy mediums, and tune variables for GPU speedups. Given that this simulator is limited by its domain, step size, and corners, near-far field compensation, thin wire, and conformal mesh features would further improve the performance. One of the findings that was most shocking is the ability to simulate any frequency without impacting the simulation time due to the program being limited by the physical domain where high resolution, high frequency simulations with the MoM solver took nearly 1.6 times as long to execute compared to the FDTD solver. This is profound since the FDTD simulator then appears to be strong for very high frequency near-field simulation of photonic and electronic systems of any size using any numerical methods. Due to this trait, FDTD developed and debugged by a knowledgeable user could be very strong tool for quantum simulations which high resolution and high frequency is required and likely could not be as easily achieved by a MoM solver. This is likely to be a topic of future research.

VII. References

[1] K. Yee, "Numerical solution of initial boundary value problems involving Maxwell's equations in isotropic media," IEEE Transactions on Antennas and Propagation, vol. 14, no. 3, pp. 302-307, May 1966.

[2] S. D. Gedney, “An anisotropic perfectly matched layer-absorbing medium for the truncation of FDTD lattices,” IEEE Transactions on Antennas and Propagation, vol. 44, pp. 1630–1639, December 1996. DOI: 10.1109/8.546249

[3] Figure 7.44 pg. 364 Pozar, D. M. (2012). Microwave engineering. Wiley.

[4] Clayton R. Paul, "Incorporation of terminal constraints in the FDTD analysis of transmission lines," IEEE Transactions on Electromagnetic Compatibility, vol, 36, no. 2, pp. 85-91, May 1994.